



Research Article

Effect of firing temperature on structural and electrical parameters of synthesized CeO₂ thick films



Rahul Dheerendra Singh¹  · Prashant Bhimrao Koli¹  · Babu Sonu Jagdale¹  · Arun Vitthal Patil²

© Springer Nature Switzerland AG 2019

Abstract

In this work, the Ceria (CeO₂) was synthesized by co-precipitation method. The thick films of synthesized CeO₂ were prepared by screen printing technique. Films were fired at 350 °C, 400 °C, 450 °C for 2 h in muffle furnace. These films were characterized by XRD to investigate the structural properties of prepared material. The XRD confirmed the single phase cerium oxide nanoparticles. Scanning electron microscopy was utilized for the morphological parameters of prepared cerium oxide nanoparticles. The cubic shaped cerium nanoparticles with various diameters were observed from SEM images. The elemental composition of ceria was studied by EDS, where the perfect elemental composition of ceria was confirmed. The Fourier transform infra red spectroscopy was employed to find out metal-oxide vibrational bands in the cerium oxide nanoparticles. The effect of firing temperature was studied for cerium oxide calcined at 350 °C, 400 °C and 450 °C nanoparticles to study the various parameters such as Grain Size, Temperature Coefficient (T_c), Stacking Fault Probability (α), Dislocation Density (ρ), Surface area, Activation Energy and RMS Microstrain (ε).

✉ Rahul Dheerendra Singh, singhrahul0910@gmail.com | ¹PG Department of Chemistry and Research Centre in Chemistry, Loknete Vyankatrao Hiray Arts, Science, and Commerce College (Affiliated to SPPU, Pune), Panchavati, Nashik, Maharashtra 422003, India. ²PG Department of Electronics and Research Centre, Loknete Vyankatrao Hiray Arts, Science, and Commerce College (Affiliated to SPPU, Pune), Panchavati, Nashik, Maharashtra 422003, India.

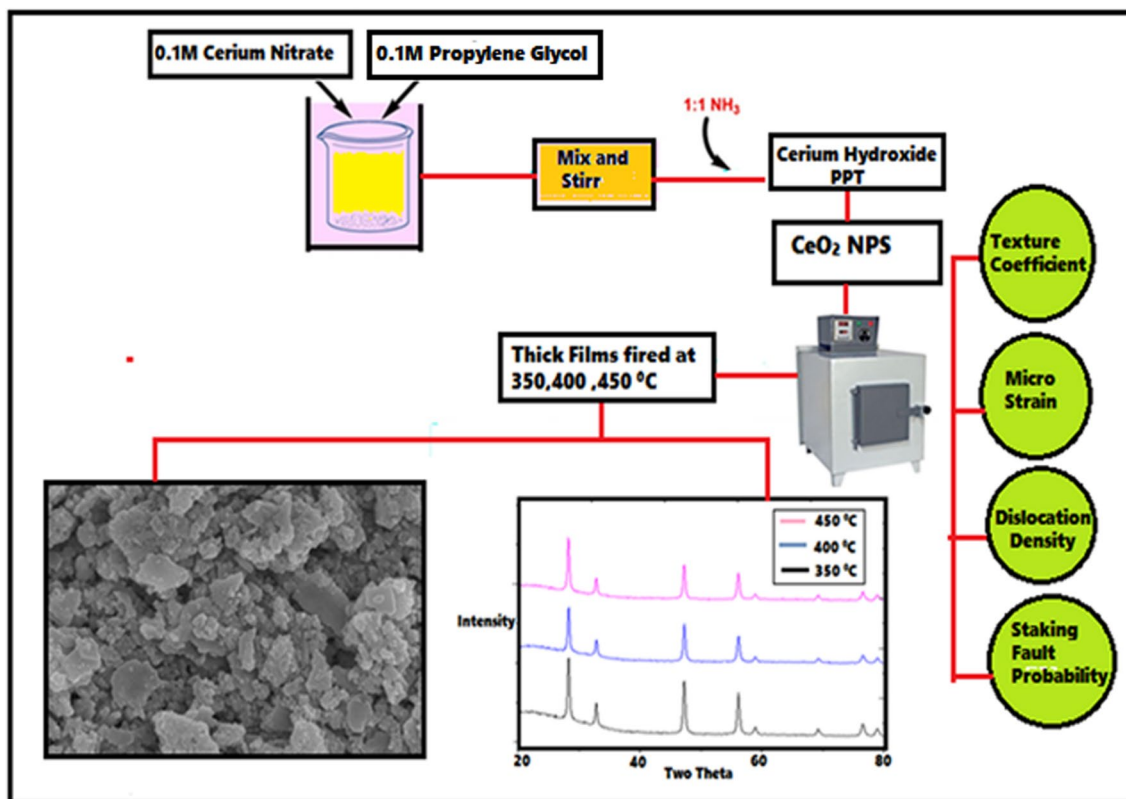


SN Applied Sciences (2019) 1:315 | <https://doi.org/10.1007/s42452-019-0246-5>

Received: 4 November 2018 / Accepted: 11 February 2019 / Published online: 7 March 2019

SN Applied Sciences
A SPRINGER NATURE journal

Graphical abstract



Keywords Ceria nanoparticles · XRD · SEM · EDS · Electrical parameters · Effect of firing temperature

1 Introduction

The nanotechnology now a day at the top edge of research due to its remarkable application in various fields of catalysis. Due to versatile application of nanotechnology, it attracted the attention of many researchers. The material science covers various applications such as homogeneous and heterogeneous catalysis, solar cells, gas sensors, SOFC (Solid oxide fuel cell), high density memory devices, bio-sensors, drug delivery mechanism, photocatalysis, green synthesis using plant extract, chemotherapy, organic conversions, waste water treatment or effluent treatment etc. [1, 2].

A wide range of materials have been synthesized for various applications of nanoscience. Generally the transition metals oxides, very efficient catalyst have been used for various applications. But now a day's use of inner transition metal oxide is a new trend in the field of catalysis, particularly lanthanum, cerium and europium oxide are extensively used materials for sensing mechanism [3, 4] The pure oxide in the form of M_2O_3 and perovskite materials are

frequently used materials. The most widely used material among lanthanide series ceria nanoparticles. Cerium possess some exceptional properties such as SOFC, oxygen ion conductor [5], solid state electrolytes for electrochemical devices, oxygen storage capacitor (OSC), sunscreen for UV absorbent, grating for chemical and mechanical planarization, hybrid solar cells [4]. Cerium oxide has a cubic fluorite structure with band gap 3.26 eV, hence cerium can be utilized as effective semiconductor due to sufficient distance between valence band and conduction band. It has lattice constant found to be 5.411 with $Fm\bar{3}m$, #225 as space group.

The common methods used for the synthesis of ceria nanoparticles are co-precipitation method, sol-gel method, forced hydrolysis, hydrothermal method, surfactant templating method, combustion method, synthesis using plant extract, Synthesis using ball grinding method. All the above listed methods are recognized method for the synthesis of various nanoparticles [6–9].

Most of the researchers have been reported the applications of synthesized nanoparticles in various filed,

particularly the inner transition metal oxides are found to be excellent catalyst in the field of sensing mechanism as sensors, transducers, electronic and magnetic applications. Especially lanthanum and cerium oxides, doped with minute concentration of inner transition metals, transition metals and some selected P-block metals enhanced the catalytical reactivity of cerium and lanthanum oxides. Researchers also reported that the lanthanum and cerium oxides are potent catalyst for sensor mechanism [10–12].

In the present research authors are highlighting the structural based properties of cerium oxide which are studied with the help of X-ray diffractometer, Scanning electron microscope (SEM), Fourier transform infra red (FT-IR) spectroscopy etc. The method of material synthesis and microstructural defects leads to change the various properties of material such as optical, physical, electrical and sometimes magnetic properties of the material. These minute changes in the material may be influence on the catalytical and desired substantial properties. Literature also reports that these minute defects leads to decrease the sensing and adsorption related properties of solid materials [13–15].

Ceria nanomaterials prepared by co-precipitation method were studied for different structural properties. These nanoparticles were extremely utilized as sensors for most of the oxidizing and reducing gases, but the microstructural investigation of ceria nanoparticles has not been reported. Thus authors are reporting this research for finding any structural defects, etymology produced in the ceria nanoparticles synthesized by co-precipitation method.

In this research paper we are reporting structural and morphological investigation of ceria nanoparticles under the influence of firing temperature effect ranging from 350 to 450 °C. The structural and morphological study involves effect on the parameters such as Grain size, Stacking fault Probability (α), Dislocation density (ρ) RMS micro-strain, surface area and activation energy [16–18].

2 Materials and methods

All the in chemicals used in synthesis are of AR grade purchased from Loba chemie, Mumbai such as $[\text{Ce}(\text{NO}_3)_3] \cdot 6\text{H}_2\text{O}$, propylene glycol, ammonia, Double purified water. The chemicals were used without further purification.

2.1 Synthesis of ceria nanoparticles by co-precipitation method

The refinement of ceria nanoparticles conjoin with; $[\text{Ce}(\text{NO}_3)_3] \cdot 6\text{H}_2\text{O}$, propylene glycol and ammonia.

Preparation of desired solutions are uniformed with double purified water, disorganized Nano-crystalline CeO_2 powder was prepared by controlled addition of aqueous ammonia to a mixture of 0.1 M aqueous solution of cerium nitrate and propylene glycol; the ratio of concentration of propylene glycol to cerium nitrate solution was kept 1:1. The special arrangement was made to add drop wise aqueous ammonia into the solution with constant stirring. After complete swiftness, the precipitated hydroxide was washed with purified water, and then pure hydroxide in a crucible was placed in a kiln for fireside (at 400 °C) about 120 min. The Phase purity and the degree of crystallinity of the resulting CeO_2 sample were monitored by XRD analysis [19, 20].

2.2 Fabrication of ceria thick films by screen printing method

The thick films of pure Ceria (CeO_2) were prepared by screen printing technique, in which the inorganic and organic ratio was kept constant as 70:30 respectively. The inorganic part comprises by pure ceria nanoparticles. Whereas organic parts reckon in with 8% BCA (Butyl Carbitol Acetate) and 92% ethyl cellulose; these compounds were assembled in mortar and pestle which has lavenment with acetone and dried [21]. BCA added drop wise in accumulated mixtures to achieve the proper pseudo-plastic phase (Thixotropic), which glutinous in nature; then applied on previously shaped glass substrate (2×1 cm) by screen printing method. The screen of nylon (40 s, mesh number 355) was used for screen printing. The standard mask size was developed on the screen by photolithography technique, after that the films were kept as it is for 15 min, then films were dried under IR lamp for 30 min [22, 23]. Finally the films were calcined under muffle furnace at 600 °C for 4 h. The pure ceria thick films are ready for characterization and further use.

3 Characterization methods

3.1 X-ray diffraction

The Structural properties of ceria thick film were analyzed by using X-ray diffraction method. The material ceria was calcined at three different temperatures 350 °C, 400 °C and 450 °C. The typical XRD spectrum of cerium oxide is as depicted in Fig. 1 the spectrum shows 2θ values from 28.302, 32.851, 47.270, 56.089, 58.889, 69.178, 76.528, 78.838, which corresponds to hkl planes as 111, 200, 220, 311, 222, 400, 331, and 420 respectively. Data obtained from XRD confirms the single phase cubic cerium oxide formation. The average particle size calculated from

Scherrer formula (Eq. 1) fired at 350 °C, 400 °C, 450 °C was 13.63 nm, 12.63 nm, 13.7 nm respectively.

$$D = \frac{K\lambda}{\beta \cos \theta} \tag{1}$$

where D is average particle size, K is constant (0.9 to 1), λ = wavelength of X-rays (1.54 Å) β is full width half maxima (FWHM) of diffracted peak, θ is the angle of diffraction. The XRD pattern of cerium oxide nanoparticles matches with the JCPDS standard number 750390.

3.2 Texture coefficient: (T_C)

Values which are obtained using Eq. (2) it has seen that T_C advice oneness for conjecturally distributed specimen; whereas T_C is larger than oneness of preferentially oriented (hkl) plane. The inferior values of T_C irradiates that, the films have poor crystallinity and this may be improved at higher firing temperature Fig. 2 shows the variation of the texture coefficient for the firing temperature ranging from 300 to

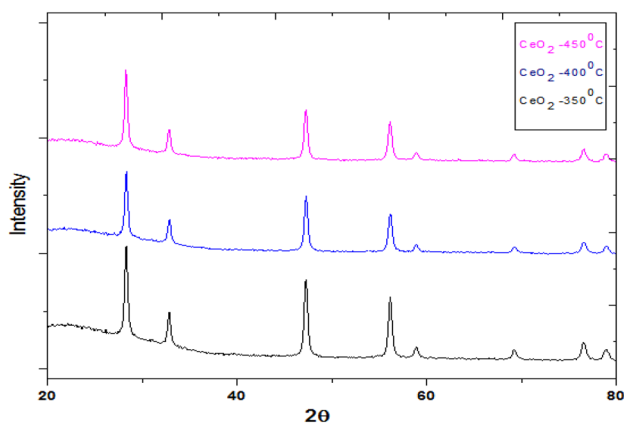


Fig. 1 XRD spectrum of prepared cerium oxide nanoparticles thick films fired at 350 °C, 400 °C, 450 °C

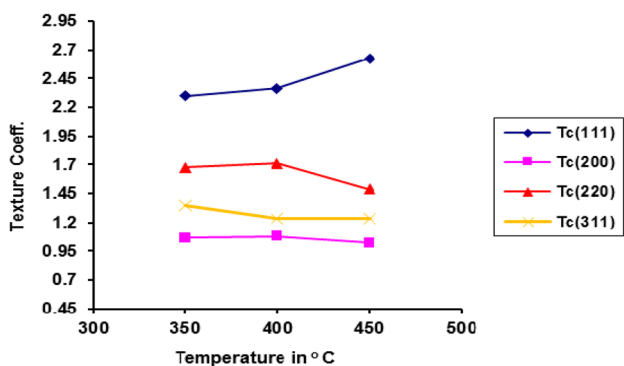


Fig. 2 Variation of texture coefficient along with the firing temperature

450 °C for (111), (200), (220), (311), planes. It is observed that the preferred orientation is (111) plane for all firing temperatures. The enhancement in preferred orientation is assigned to maximum number of grains belongs to this orientation [24, 25].

$$T_C[hkl] = \frac{\frac{I[hkl]}{I_0[hkl]}}{\frac{1}{N} \sum \frac{I[hkl]}{I_0[hkl]}} \tag{2}$$

3.3 Stacking fault probability (α)

Stacking fault probability arises when one atomic plane sets out of series than others to start piling up; on the other hand lattice remains surpassing. Due to stacking fault only the position of peak shows variation from JCPDS for its corresponding sample. The stacking fault is most of the time considered as a planar defect. As the defect is associated with shifting of the planes two theta values of XRD data. When the particular solid material is calcined at different temperatures these types of are more pronounced and can be identified by the XRD analysis. Whenever the order of stacking fault is higher in a particular material then the exact cross slip dislocation can be found. Whereas at lower temperature the perfect disorder is cannot be observed but small dislocation can be seen. The diagram for preferred plane orientation for stacking fault probability is as shown in Fig. 3.

$$\alpha = \frac{2\pi^2 \Delta(2\theta)}{45\sqrt{3} \tan \theta_{111}} \tag{3}$$

3.4 Micro strain

Broaden X-ray diffracted line frame work mainly observed by non-prototype of instrument, wavelength dispersion and microstructural flaw in the crystal. Out of these three the microstructural flaw is sectioned into size broadening and strain broadening. Size broadening results due to confined size of domain occupy by stacking faults or by other flaws which are irrelevant with each other on the other hand strain broadening is conveyed by altered position of the atom with respect to their cited lattice parameter. An identical compressive or tensile strain (microstrain) is outcome of peak shift of the X-ray diffraction lines, whereas an identical stastical separation of tensile and compressive strain together outcomes into broaden diffraction lines (microstrain). The detailed method of for determining microstrain by X-ray diffraction lines are depicted by Williamson and hall plot. It is reputed scheme which explains qualitative knowledge of anisotropy broadening. Here, Slope of a plot of ($\beta \cos \theta / \lambda$) versus ($2 \sin \theta / \lambda$) gives the value

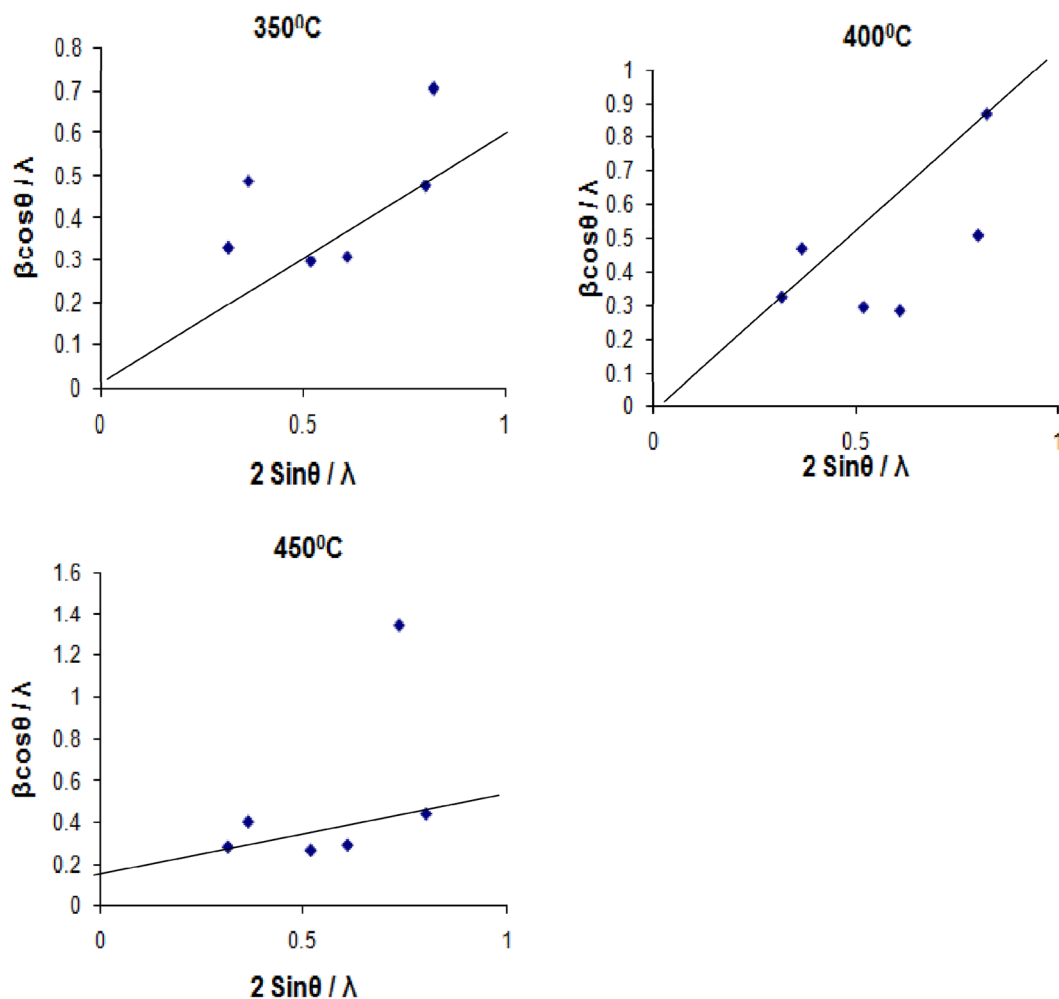


Fig. 3 Williamson–Hall plots for CeO₂ thick films with different deformations at different firing temperatures

Table 1 Variation of structural parameters with firing temperature

Firing Temp. °C	Crystalline (grain) size, D nm (XRD)	Particle size, d nm (SEM)	Specific surface area in m ² /g	Dislocation density, ρ × 10 ¹³ Lines/cm ²	Microstrain, e	Stacking fault probability, α
350	13.63	250	3.328	5.904	0.9129	0.2482
400	12.63	300	2.772	4.912	0.8042	0.2482
450	13.7	325	2.218	3.948	0.7195	0.3031

of the RMS Microstrain Fig. 3 depicts the Williamson-Hall plot for CeO₂ thick films with different deformation from planes (111) to (420) at different calcined temperature, Here in Fig. 3 the points are scattered then microstrain is RMS that is if (βcos θ/λ) is nonmonotonic function of (2sin θ/λ), the broadening is termed anisotropic. The RMS microstrain calculated at different firing temperatures indicate a decreasing trend with firing temperature is given in Table 1 (Figs. 4, 5).

$$\rho = \sqrt{12}(e^2)^{1/2}/dD \tag{4}$$

3.5 Scanning electron microscopy (SEM)

The SEM images of prepared CeO₂ material is as depicted in Fig. 6. The material was calcined at three different temperatures at 350 °C, 400 °C, 450 °C. From SEM images it

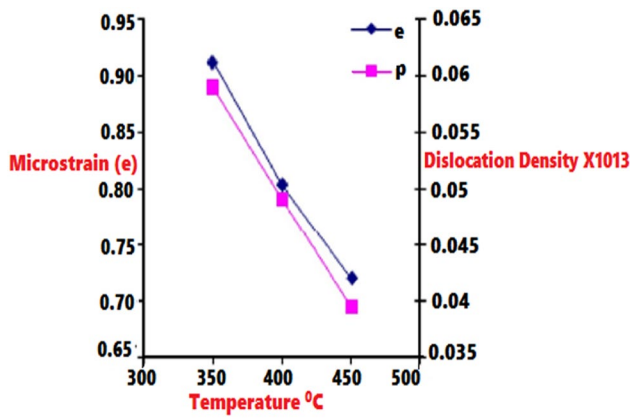


Fig. 4 Variation of microstrain (e) and dislocation density (ρ) with firing temperature

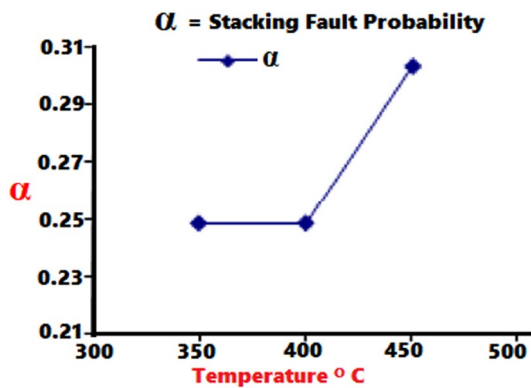


Fig. 5 Variation of stacking fault probability with firing temperature

is found that the crystal size of ceria nanoparticles is increased with rise in temperature. The various size ceria nanoparticles can be seen from the SEM images as shown in Fig. 6. The calculated particle size of crystalline ceria particles is as shown in Table 1. Due to effect of calcination temperature on the nanoparticles, the atomic mobility if increase. This leads to movement of atoms to more comfortable sites on the surface such voids, interstitial positions, grain boundaries etc. The ceria nanoparticles found to be very effectively adhered on the film surface. As well as the surface area and homogeneous surface of ceria nanoparticles is found to be very effective in electrical conductivity and sensing mechanism (Table 2).

$$S_w = \frac{6}{\rho \times d} \tag{5}$$

3.6 Energy dispersive spectroscopy (EDS)

The cerium oxide nanoparticles were characterized by EDS to know the elemental composition of prepared material. The EDS spectrum of prepared CeO₂ calcined at 350 °C, 400 °C, 450 °C is as depicted in Fig. 7 from which the perfect elemental composition of cerium oxide is can be seen. The mass percentage of cerium is found to be decrease with increase in temperature as the oxygen mass percentage was increased with increase in temperature. This reverse trend is observed in case of Ceria nanoparticles is due to the inherent SOFC (Solid oxide fuel cell), OSC (oxygen storage capacitor) properties of ceria. The effect of firing temperature on the elemental composition is clearly can be seen from the following data represented in Table 3.

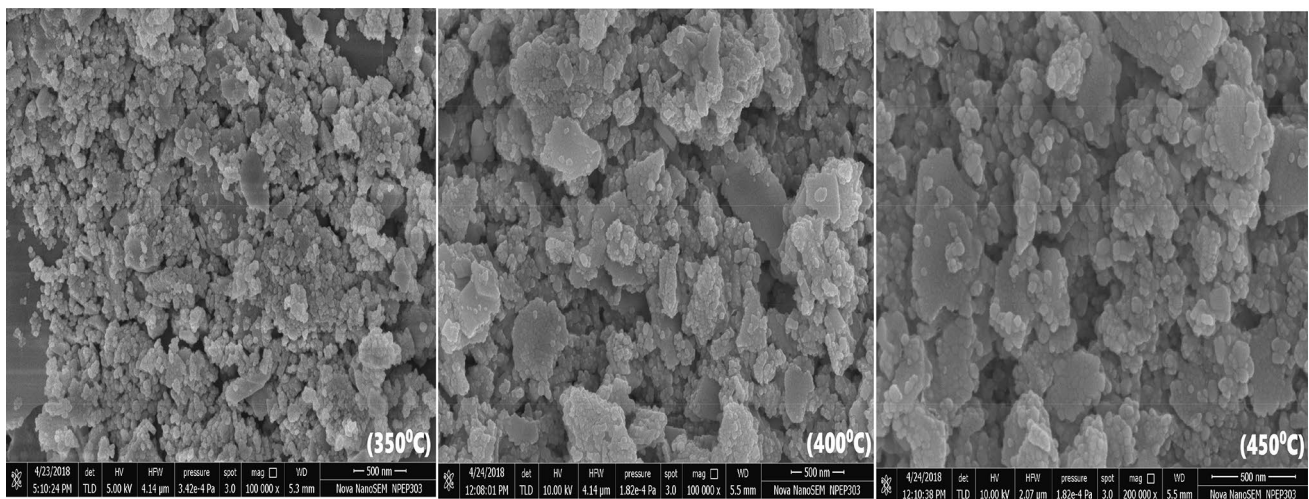
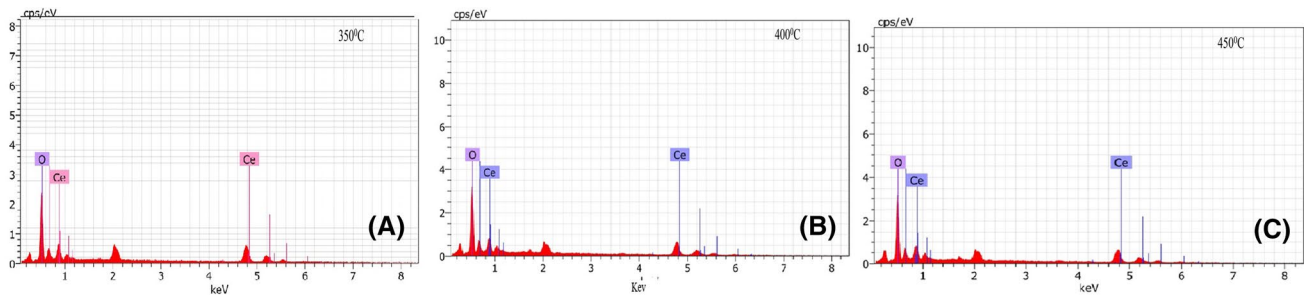


Fig. 6 SEM images of prepared cerium oxide nanoparticles thick films fired at 350 °C, 400 °C, 450 °C

Table 2 Surface area and particle size calculated using BET method for spherical particles from SEM data

Functioning material	Firing temperature °C	Crystallite (grain) size, D nm (XRD)	Particle size, d nm (SEM)	Specific surface area in gm/cm ³
Pure CeO ₂	350	13.63	250	33.28 × 10 ³
Pure CeO ₂	400	12.63	300	27.72 × 10 ³
Pure CeO ₂	450	13.7	325	22.18 × 10 ³

**Fig. 7** EDS images of prepared cerium oxide nanoparticles thick films fired at **a** 350 °C, **b** 400 °C, **c** 450 °C**Table 3** Composition of CeO₂ thick films at different firing temperatures 350 °C, 400 °C, 450 °C

Firing temperature (°C)	Element	Normal wt %	Atomic wt %
350	Ce	83.21	36.13
	O	16.79	63.87
400	Ce	82.13	34.42
	O	17.87	65.58
450	Ce	79.43	30.60
	O	20.57	69.40

3.7 Infra-red spectroscopy

The infra-red spectroscopy normally enables the chemical bonding formation in the compounds. These bonding can be detected in terms of stretching and bending mode of frequencies. The metal oxide linkages have a typical stretch in IR radiations and hence these unique frequencies can be detected by using vibrational stretching bands. Cerium oxide is fluorite type material with cubic arrangement. The typical IR spectrum of prepared ceria nanoparticles is as shown in Fig. 8, where the different frequency bands can be observed. The typical Ce–O stretching vibration of the material calcined at 350 °C, 400 °C, 450 °C found at 794.30 cm⁻¹, 764 cm⁻¹ and 763.6 Cm⁻¹ respectively. Where as deformed water stretching is found at 1627.50 cm⁻¹, 1596.9 cm⁻¹ and 1591.5 cm⁻¹ respectively for cerium oxide calcined at 350 °C, 400 °C, 450 °C. The broad peaks in each cerium oxide calcined at

different temperatures is typically found at 3437.3, 3453.3, 3361.2.

4 Conclusions

This research work has been attributed to the synthesis of Ceria nanoparticles by a cost effective co-precipitation method. Subsequently the screen printed thick films of ceria nanoparticles were applied for the investigation of some structural parameters such as Microstrain, dislocation density, RMS, texture coefficient and stacking fault probability. The crystallographic parameters as mention above found to be influenced due to increase temperature effect. The texture coefficient and stacking fault probability was studied and discussed for the major diffraction line such as (111). The effect of temperature on various microstructural properties studied in the present research, (represented in Table 1). The particle size reported from SEM found to be increased due to increase in grain size at higher temperature. The specific surface area is observed to be decrease due to increase in grain size, as there is an inverse relation between grain size and surface area. The planar defect stacking fault probability is increased with the rise in temperature probably due to enhancement of randomness at higher temperature. As all these parameters are closely related to each other regarding the structural aspects of the materials. The study of such parameters can be useful while working with the structural and morphological investigations of the materials.

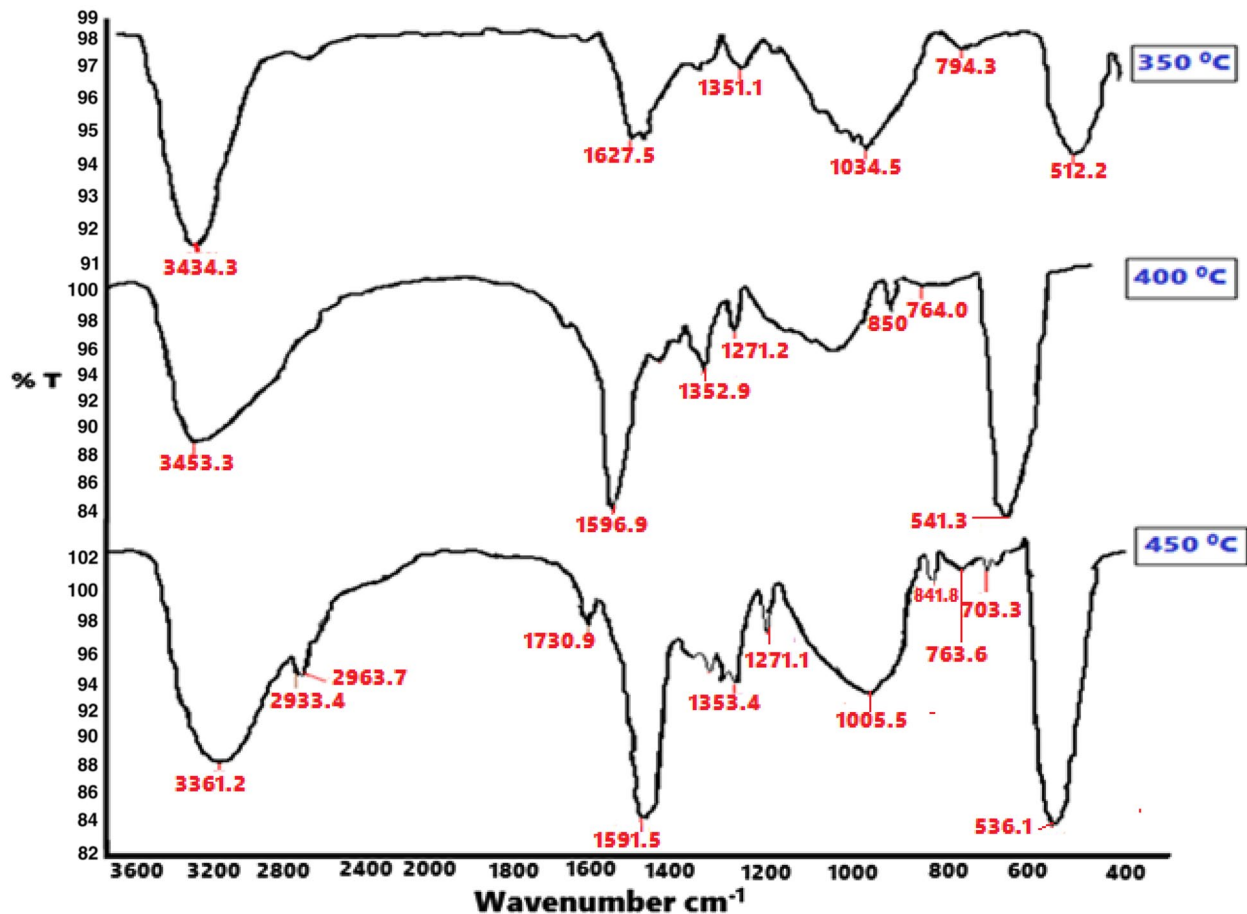


Fig. 8 FT-IR spectrum of prepared cerium oxide thick films fired at 350 °C, 400 °C, 450 °C

Acknowledgements Authors are gratefully acknowledged to the SAIF UDCT, Jalgaon (M.S) for XRD, SEM study. Authors are thankful to SAIF IIT Bombay for TEM and EDS analysis as well as SAIF Chandigarh (Punjab University) for FT-IR study. Authors are very thankful to Department of Chemistry, L.V.H. College, Panchavati, Nashik and Department of electronics L.V.H. College, Panchavati, Nashik.

Compliance with ethical standards

Conflict of interest The authors declare that they have no conflict of interest.

References

- Tang M-H, Zhou Y-C, Zheng X-J, Wei Q-P, Cheng C-P, Ye Z, Hu Z-S (2007) Microstructure and electrical properties of CeO₂ ultra-thin films for MFIS feram Applications. *Trans Nonferr Met Soc* 17:5741–5746
- Zhang L, Fang Q, Huang Y, Xu K, Chu PK, Ma F (2018) Oxygen vacancy enhanced gas sensing performance of CeO₂ graphene heterostructure at room temperature. *Anal Chem.* <https://doi.org/10.1021/acs.analchem.8b01768>
- Dhall A, Self W (2018) Cerium oxide nanoparticles: a brief review of their synthesis methods and biomedical applications. *Anti-oxidants.* <https://doi.org/10.3390/antiox7080097>
- Farahmandjou M, Zarinkamar M, Firoozabadi TP (2016) Synthesis of cerium oxide (CeO₂) nanoparticles using simple co-precipitation method. *Revista Mexicana de Física* 62:496–499
- Acharya SA, Gaikwad VM, Sathe V, Kulkarni SK (2014) Influence of gadolinium doping on the structure and defects of ceria under fuel cell operating temperature. *Appl Phys Lett* 104:113508. <https://doi.org/10.1063/1.4869116>
- De Marzi L, Monaco A, De Lapuente J, Ramos D, Borrás M, Di Gioacchino M, Santucci S, Poma A (2013) Cytotoxicity and genotoxicity of ceria nanoparticles on different cell lines in vitro. *Mol Sci* 14:3065–3077. <https://doi.org/10.3390/ijms14023065>
- Hu C, Zhang Z, Liu H, Gao P, Wang ZL (2006) Direct synthesis and structure characterization of ultrafine CeO₂ Nanoparticles. *Nanotechnology* 17:5983–5987. <https://doi.org/10.1088/0957-4484/17/24/013>
- Chen MY, Zu XT, Xiang X, Zhang HL (2007) Effects of ion irradiation and annealing on optical and structural properties of CeO₂ films on sapphire. *Phys B* 389:263–268. <https://doi.org/10.1016/j.physb.2006.06.162>
- Elidrissi B, Addou M, Regragui M, Monty C, Bougrine A, Kachouane A (2000) Structural and optical properties of CeO₂ thin films prepared by spray pyrolysis. *Thin Solid Films* 379:23–27

- Guzman J, Carretin S, Corma A (2005) Spectroscopic evidence for the supply of reactive oxygen during CO oxidation catalyzed by gold supported on nano crystalline CeO₂. *J Am Chem Soc* 127:3286–3287
- Kek-Merl D, Lappalainen J, Tuller HL (2006) Electrical properties of nanocrystalline CeO₂ thin films deposited by in situ pulsed laser deposition. *J Electrochem Soc* 153(3):J15–J20
- Liu YH, Zuo JC, Ren XF, Yong L (2014) Synthesis and characterization of cerium oxide (CeO₂) nanoparticles by the precipitation method. *Metalurgija* 53:463–465
- Qi G, Yang RT, Chang R (2004) MnOx-CeO₂ mixed oxides prepared by co-precipitation for selective catalytic reduction of NO with NH₃ at low temperatures. *Appl Catal B* 51:93–106
- Si R, Flytzani-Stephanopoulos M (2008) Shape and crystal-plane effects of nanoscale ceria on the activity of Au-CeO₂ catalysts for the water–gas shift reaction. *Angew Chem* 120:2926–2929
- Akla AA, Mahmoud SA, Al-Shomar SM, Hassanien AS (2018) Improving microstructural properties and minimizing crystal imperfections of nanocrystalline Cu₂O thin films of different solution molarities for solar cell applications. *Mater Sci Semicond Process* 74:183–192. <https://doi.org/10.1016/j.mssp.2017.10.007>
- Trovarelli A (1996) Catalytic properties of ceria and CeO₂-containing materials. *Catal Rev* 38(4):439–520. <https://doi.org/10.1080/01614949608006464>
- Xiong Y-P, Kishimoto H, Yamaji K, Yoshinaga M, Horita T, Brito ME, Yokokawa H (2011) Electronic conductivity of pure ceria. *Solid State Ionics* 192:476–479. <https://doi.org/10.1016/j.ssi.2010.07.017>
- Patil AV, Dighavkar CG, Sonawane SK, Shinde UP, Patil SJ, Borse RY (2010) Study of microstructural parameters of screen printed ZnO thick film sensors. *Sens Transducers* 117(6):62–70
- Kanakaraju S, Mohana S, Sood AK (1997) Optical and structural properties of reactive ion beam sputter deposited CeO₂ films. *Thin Solid Films* 305:191–195
- Kasipar J, Fornasiero P, Graziani M (1999) Use of CeO₂-based oxides in the three-way catalysis. *Catal Today* 50:285–298
- Borhade AV, Tope DR, Agashe JA (2018) Synthesis, characterization and gas sensing performance of nanocrystalline ZrO₂, 5%Y/ZrO₂ and Ag–5%Y/ZrO₂ catalyst. *J Mater Sci Mater Electron* 29:7551–7561
- Patil AV, Dighavkar CG, Sonawane SK, Patil SJ, Borse RY (2009) Effect of firing temperature on electrical and structural characteristics of screen printed ZnO thick films. *Optoelectr Adv Mater Rapid Commun* 3(9):879–883
- Patil AV, Dighavkar CG, Sonawane SK, Patil SJJ, Borse RY (2009) Formulation and characterization of Cr₂O₃ doped ZnO thick films as H₂S gas sensor. *Sensors & Transducers* 108(9):189–197
- Schuler T, Aegerter MA (1999) Optical, electrical and structural properties of sol gel ZnO: Al coatings. *Thin Solid Films* 351(1–2):125–131. [https://doi.org/10.1016/S0040-6090\(99\)00211-4](https://doi.org/10.1016/S0040-6090(99)00211-4)
- Durrani SMA, Al-Kuhaili MF, Bakhtiari IA (2009) Carbon monoxide gas-sensing properties of electron-beam deposited cerium oxide thin films. *Sens Actuators B* 134(2008):934–939. <https://doi.org/10.1016/j.snb.2008.06.049>

Publisher's Note Springer Nature remains neutral with regard to jurisdictional claims in published maps and institutional affiliations.